ORIGINAL ARTICLE

Targeted Gold Nanoparticles for Molecular CT Imaging of Breast Cancer: An In-Vitro Study

Navid Kheradmand [1], Omid Talaee [2], Fatemeh Tabatabaee [3], Vahideh Alvandi [4], Emad Khoshdel [5,6], Parizad Ghadimi [7], Mustafa Çaglar [1*]

[1] *Department of Health Physics, Graduate School of Health Sciences, İstanbul Medipol University, İstanbul, Türkiye*

[2] *Department of Nuclear Engineering, Faculty of Mechanical Engineering, University of Shiraz, Shiraz, Iran*

[3] *Department of Medical Physics, School of Medicine, Tabriz University of Medical Sciences, Tabriz, Iran*

[4] *Department of Physics, Faculty of Sciences, Razi University, Kermanshah, Iran*

[5] *Department of Medical Physics, Faculty of Medicine, Mashhad University of Medical Sciences, Mashhad, Iran*

[6] *Student Research Committee, Mashhad University of Medical Sciences, Mashhad, Iran*

[7] *Department of Medical Physics and Radiology, Faculty of Medicine, North Khorasan University of Medical Sciences, Bojnurd, Iran*

*Corresponding Author: Mustafa Çaglar
Email: mcaglar@medipol.edu.tr

Received: 26 March 2024 / Accepted: 19 May 2024

Abstract

Purpose: The incorporation of Nanoparticles (NPs) in Computed Tomography (CT) imaging significantly enhances the contrast, clarity, and sensitivity of CT scans, leading to a substantial improvement in the accuracy and reliability of diagnostic information obtained from the images. The objective of the current research was to investigate the application of gold (Au) NPs in enhancing the imaging capabilities of Breast Cancer (BC) cells.

Materials and Methods: Au NPs were synthesized by loading Trastuzumab (TZ) on PEGylated Au NPs. Firstly, Au NPs were produced and coated with PEG-SH to form PEG-Au NPs. Next, TZ was coupled with OPSS-PEG-SVA to enable its attachment to the PEG-Au NPs. The resulting NPs were characterized for their structure, size, and morphology using standard analytical techniques. To assess the potential of the developed NPs for CT scan imaging of BC cells, SKBr-3 cells were treated with Au NPs and TZ-PEG-Au NPs. Additionally, the cytotoxicity of the NPs was evaluated with the MTT technique.

Results: The SEM and TEM analyses revealed that the synthesized NPs exhibited a spherical shape and displayed a relatively uniform size distribution (approximately 45 nm). The results showed that the developed Au NPs have acceptable biocompatibility and superior X-ray attenuation properties compared to a commonly used contrast agent.

Conclusion: Based on our results, it can be concluded that the proposed TZ- Polyethylene Glycol-Au NPs are suitable for CT imaging of BC cells.

Keywords: Au Nanoparticles; Polyethylene Glycol; Molecular Imaging; Computed Tomography; Breast Cancer Cells.

DOI: https://doi.org/10.18502/fbt.v12i3.19210

1. Introduction

Breast Cancer (BC) is the primary source of cancer-related fatalities among women on a global scale. Premature detection and accurate imaging techniques play a vital role in successful patient outcomes by empowering timely diagnosis, staging, and treatment planning [1]. Mammography, ultrasound, and Magnetic Resonance Imaging (MRI) are the chief imaging methods used for BC screening, diagnosis, and monitoring [2]. Recent research in the biology of BC successfully modeled cancer cell responses to various therapeutic approaches, leading to more precise diagnosis and treatment strategies [3, 4]. However, with advances in technology, Computed Tomography (CT) scans have also gained a role in BC management. The CT scans are used for staging, detecting metastases, and treatment planning [5]. In recent years, the field of molecular imaging has emerged as an encouraging approach for non-invasive visualization and characterization of cancer at the molecular level. This technique involves the use of molecularly targeted imaging agents that selectively bind to specific biomarkers overexpressed on cancer cells, providing enhanced sensitivity and specificity for tumor detection [6].

Nanoparticles (NPs) are highly promising for molecular imaging due to their unique properties [7]. They can enhance contrast, target specific molecules, enable multimodal imaging [8], and serve as theranostic agents [9, 10]. With biocompatibility and the ability to image at cellular and molecular levels, NPs have the potential to revolutionize disease diagnosis, treatment guidance, and patient care [11, 12].

Gold (Au) NPs have garnered significant attention in the field of molecular imaging due to their exclusive physicochemical properties, including tunable size, shape-dependent optical properties, and ease of surface functionalization [13]. These properties make Au NPs excellent candidates for targeted imaging agents [14]. Li *et al.* investigated the development of a multifunctional Au NP as a Contrast Agent (CA) for dual-modality imaging of BC cells. The researchers used dendrimers modified with Polyethylene Glycol (PEG) to synthesize the Au NPs. The resulting multifunctional dendrimer-entrapped Au NPs were used for MRI and CT imaging of BC cells. Equally MR and CT images demonstrated effective imaging of the BC cells [15]. Rayavarapu *et al.* conducted a study in which they synthesized and characterized Au NPs, both spheres and rods, for use as CAs in optical imaging techniques. They successfully bio-conjugated these Nano-rods with HER-81 antibodies, known for their high affinity to epidermal growth factor receptor-2 (HER-2) receptors expressed by SKBr-3 breast carcinoma cells. In in-vitro studies, it was observed that the targeting functionality of the antibody moiety remained effective, demonstrating the potential of these nanorods for targeted imaging of HER-2 positive BC cells [16].

Through the conjugation of Au NPs with specific targeting agents like antibodies, peptides, or small molecules, it becomes feasible to actively target cancer cells. This approach offers several benefits, including enhanced imaging contrast and improved accuracy in detecting and visualizing cancer cells [17]. HER-2 is a cell surface receptor that is overexpressed in approximately 20-30% of BC cases [18]. HER-2 overexpression is associated with aggressive tumor behavior and poor prognosis. Trastuzumab (TZ), a monoclonal antibody, specifically targets HER-2 and has been widely used for the treatment of HER-2-positive BC [19]. Capitalizing on the specificity and binding affinity of TZ, it is possible to develop HER-2 targeted Au NPs for molecular imaging of BC [20]. Abdollahi *et al.* assessed the effect of molecularly targeted Au NPs on tumor radio-sensitization of SKBr-3 BC cells. They synthesized the HER-2-targeted Au NPs by conjugating TZ to PEG-Au NPs. Results exhibited that the targeted TZ-PEG-Au NPs meaningfully enhanced breast cell uptake [13]. Similarly, Reuveni *et al.* demonstrated the feasibility of using clinical CT for cancer diagnosis based on molecular markers rather than anatomical structures. They used anti-Epidermal Growth Factor Receptor (EGFR) conjugated Au NPs in mice with squamous cell carcinoma. The NPs enriched the visibility of a trivial tumor that was otherwise untraceable by CT. Active tumor targeting with the NPs proved to be more effective and specific than passive targeting [21].

We aimed to synthesize and characterize HER-2 targeted Au NPs and evaluate their effectiveness for CT molecular imaging of BC cells. The synthesis of HER-2 targeted Au NPs involved the conjugation of TZ to PEGylated Au NPs, which provide stability and biocompatibility to the NPs.

In this study, the central hypothesis is that the synthesis and characterization of TZ-conjugated Au NPs will result in targeted contrast agents with suitable properties for enhancing the molecular imaging capabilities of BC cells using CT scans. Therefore, the current study introduced a

novel approach for enhancing the imaging capabilities of BC cells using Au NPs in CT scans. The synthesized TZ-PEG-Au NPs specifically target breast cancer cells expressing HER-2 receptors, providing a promising avenue for molecular imaging and potential applications in cancer treatment as a theranostic agent.

2. Materials and Methods

2.1. 2.1. Materials

The study utilized various materials, including perchloric acid ($HClO_4$), DMSO, sodium citrate dihydrate, ammonia solution, and HAuCl4 sourced from Merck Chemicals. OPSS-PEG-SVA with a molecular weight of 5 kDa was achieved from Laysan Bio. The experiments were conducted using distilled water.

2.2. Synthesis of Au NPs

The citrate chemical reduction manner, as defined by Anshup *et al.*, was employed in this study to synthesize the Au NPs [22]. The procedure involved adding 0.02 g of HAuCl4 to 10 mg of water. The subsequent HAuCl4 solution was mixed with 90 ml of water in a round bottom flask and placed on a magnetic stirrer. Next, sodium citrate was introduced into the heated solution, resulting in a noticeable color transformation from a pale yellow shade to a deep red hue. The produced NPs were subsequently separated using filter paper and underwent centrifugation for further purification. In order to stabilize the NPs, a 0.2 ml volume of a 4% w/v PEG solution was added to a 15 ml solution of the Au NPs. The mixture was stirred for 4 hours at room temperature.

2.3. Preparation of TZ-Conjugated PEGylated Au NPs

To covalently bind the immune-conjugates to Au NPs, the PEG linker was utilized, taking advantage of the strong Au-thiol interaction. The connection between the Au NPs and the TZ drug involved PEGylation of TZ initially. To accomplish this, TZ (2 µg/µL) dissolved in PBS at a pH of 6.0 was reacted with OPSS-PEG-SVA. Following the reaction, the conjugates were filtered, and buffer substitution into PBS at a pH of 7.5 was performed. This was achieved using ultrafiltration with a Vivaspin filter featuring a 30 kDa molecular weight cutoff. To bind TZ-PEG-OPSS to Au NPs, several steps were followed. First, 80 µL of 250 µM PEG-SH was added to 2 mL of NPs (2 mg/mL). Then, 100 µg of TZ-PEG in PBS, pH 7.5, was immediately added, and the mixture was allowed to react for 60 minutes at 4°C. The final NPs were purified by placing them near a stable magnet at 4°C for the whole day [13].

2.4. Characterization of NPs

The structure and size of the synthesized NPs were examined using a JEM-1400 microscope from JEOL (Peabody, MA, USA) through Transmission Electron Microscopy (TEM) and Scanning Electron Microscopy (SEM). The acquired images were subjected to analysis using Image J software. To analyze the chemical composition, Fourier-Transform Infrared Spectroscopy (FTIR) spectra were recorded using a Shimadzu Prestige-21 spectrometer (Shimadzu Corp., Kyoto, JP). The spectra were collected in the range of 4000 cm^{-1} to 400 cm^{-1}, allowing for the identification of specific functional groups and verification of the accurate synthesis of PEG-Au NPs. Furthermore, the successful synthesis of PEG-Au NPs was confirmed using ultraviolet-visible (UV-Vis) spectroscopy.

2.5. Cell Uptake Test

Fluorescence microscopy (BD FACSCalibur, San Jose, CA, USA) was used to evaluate the cellular uptake and subcellular delivery of Au NPs and TZ-PEG-Au NPs. The assessment was based on the fluorescence intensity observed.

In the process of preparing rhodamine-labeled Au NPs and TZ-PEG-Au NPs, a concentrated solution of rhodamine is first created by dissolving 5 mg of the fluorescent dye in 1 mL of DMSO. Subsequently, suspensions of Au NPs and TZ-PEG-Au NPs are prepared, with each suspension containing 1 mL at a concentration of 1 mg/mL. To incorporate the rhodamine into the NPs, 50 µL of the rhodamine solution is added to each suspension, followed by the addition of 500 µL of 1 M sodium carbonate buffer. The resulting suspensions are then stirred for 20 hours, allowing sufficient time for the rhodamine to bind to the surfaces of the Au NPs and TZ-PEG-Au NPs.

These rhodamine-labeled NPs can be utilized in fluorescence microscopy to investigate cellular uptake and subcellular delivery.

Cells were seeded onto six-well plates at a density of 1.5×10^4 cells per plate for the cellular uptake experiments. Once the cells reached 80% confluence, they were treated with rhodamine-labeled TZ-PEG-Au NPs and Au NPs. The specific concentrations and exposure times may vary based on the experimental design. Following the incubation period, which lasted for 4 hours after treating the cells with SKBr-3 cell lines, the cells were trypsinized to detach them from the plate surface. Then, the cells were washed with PBS to remove any residual NPs or external particles. By considering the groups at different time points, the uptake kinetics of the rhodamine-labeled TZ-PEG-Au NPs and Au NPs could be examined. This approach allows researchers to investigate the internalization processes and cellular uptake mechanisms over specific time intervals, providing valuable insights into the behavior and interactions of the NPs with the SKBr-3 cells.

2.6. MTT Assay

To measure the cell cytotoxicity of NP samples, the MTT assay was employed. The following steps were carried out: samples were planted into 96-well plates at a density of 1×10^5 cells per well and incubated for one day to allow them to adhere and grow. Diverse concentrations of NPs were added to the wells and incubated with the cells for 24 hours to evaluate the dose-dependent cytotoxicity. During this time, viable cells converted the MTT reagent into formazan crystals. To assess the cell viability and determine the Optical Density (OD) of each well, an ELISA plate reader was employed. The measurements were performed at a wavelength of 570 nm, which is commonly used for assessing the metabolic activity of cells and indicative of their viability. The absorbance readings indicate the metabolic activity of the cells and can be used to determine cell viability. The assay and cell viability measurements were repeated three times to ensure the reliability and accuracy of the results. In each repetition, cells were treated with varying concentrations of the TZ, Au NPs, and TZ-PEG-Au NPs samples.

2.7. X-Ray attenuation of Au NPs and Omnipaque

In the study, the X-ray attenuation properties of the final NPs and the clinically used iodine-based CT CA, iohexol 300, were compared. Solutions with varying concentrations of the NPs and iohexol 300 were prepared and placed in 0.5 ml Eppendorf tubes. These tubes were then inserted into a CT phantom for imaging purposes. CT scan imaging was performed using a 32-slice clinical CT scan system (VCT, GE Healthcare). The CT scans allowed for the visualization and quantitative analysis of the X-ray attenuation abilities of the solutions. We utilized the following working factors: tube potentials of 80, 120, and 140 kVp, tube current set at 250 mA, an exposure time of 1000 ms, a slice thickness of 0.625 mm, a scan field of view of 250 × 250 mm, a display FOV of 130 × 130 mm, and a pitch of 1. Subsequently, CT images of the samples were obtained, and a uniform region of interest (ROI) was located on each image. X-ray attenuation values in Hounsfield units (HU) were estimated for the final NPs and Omnipaque by analyzing the ROI on the CT images. This technique was performed for all the samples to compare their X-ray attenuation properties.

2.8. Statistical Analysis

In the statistical analysis of the experimental data, a one-way analysis of variance test was employed. The ANOVA test allows for the comparison of means across multiple groups or treatments. To assess whether the observed differences in the data were statistically significant, a significance level of 0.05 (a P-value of 0.05) was taken into consideration.

3. Results

In the synthesis and characterization of the nano-complex, Au NPs were produced under specific conditions following established protocols as shown in Figure 1. To enable targeted delivery, a cross-linker was applied to bind PEG chains to TZ, resulting in the covalent attachment of PEGylated TZ to the surface of the Au NPs (Figure 1a).

UV-vis spectroscopy and FTIR spectroscopy were also performed. UV-vis spectroscopy allows for the

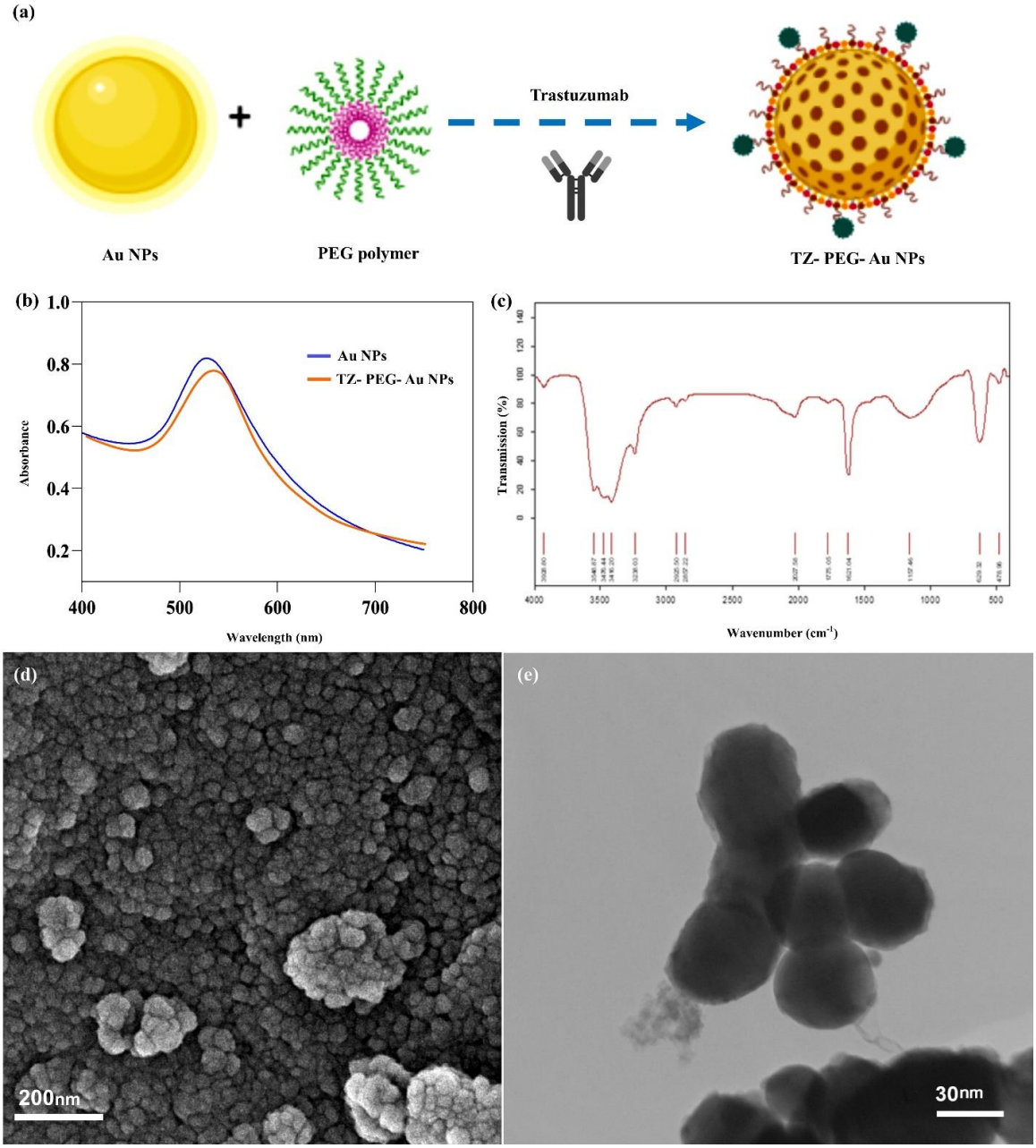

Figure 1. Characterization of TZ labeled PEGylated Au NPs. **(a)** Schematic illustration showing the synthesis of TZ-PEGylated Au NPs, **(b)** Ultraviolet-visible (UV-vis) spectroscopy of the Au NPs and PEGylated Au NPs, **(c)** Fourier transform infrared (FTIR) spectra of Au NPs, **(d)** High-resolution scanning electron microscopy (SEM) image of Au NPs, and **(e)** Transmission electron microscopy (TEM) image of Au NPs. Au (gold), PEG (polyethylene glycol), TZ (trastuzumab) and NPs (nanoparticles)

analysis of the NPs' absorption and scattering properties, particularly in the visible range (Figure 1b). FTIR spectroscopy provides valuable information about molecular interactions and functional groups present in the compound. In Figure 1c, the FTIR spectra of the Au NPs are shown, highlighting the characteristic peaks corresponding to the crystallographic planes of Au, such as Au (111), (200), (220), and (311). To confirm the proper formation of the NPs and assess their key characteristics as a contrast enhancer in CT scans, several analytical techniques were employed. TEM and SEM imaging techniques were utilized to examine the form and size of the NPs, providing detailed visual information about their structure (Figure 1d and 1e). The SEM and TEM images of the final synthesized NPs revealed a spherical structure. The images provided visual evidence that the NPs exhibit a uniform and spherical shape. Additionally, the characterization analysis indicated that the average diameter of the NPs is approximately 45

nm. These comprehensive characterization techniques collectively confirm the successful synthesis of Au NPs.

3.1. Cell Uptake Test

The cellular uptake experiment examined the uptake of the developed NPs in SKBr-3 cells using fluorescence microscopy. The results, as shown in Figure 2a, 2b, demonstrated that the TZ-PEG-Au NPs exhibited enhanced cellular absorption and targeting capabilities compared to the NPs without surface modification (Au NPs). The improved uptake of the TZ-PEG-Au NPs in the BC cell line indicates the effectiveness of TZ as a targeting ligand, allowing for specific binding to the HER-2 receptors on SKBr-3 cells (Figure 2b). This finding suggests that surface modification with TZ enhances the cellular uptake and potential targeting of the NPs in BC cells.

3.2. Cytotoxicity of Au and TZ-PEG-Au NPs

In the cell viability experiment, both MCF-10A and SKBr-3 cells were exposed to Au and TZ-PEG-Au NPs at different concentrations for 24 and 48 hours. Figure 3a, 3b) displayed the results of this experiment. It was observed that both cell lines, MCF-10A and SKBr-3, exhibited high cell viability even at doses up to 300 µM of the NPs. This suggests that the NPs did not significantly impact the viability of the cells at the tested concentrations and time points. The high cell viability indicates good biocompatibility and suggests that the NPs have minimal cytotoxic effects on the tested cell lines within the tested dosage range.

3.3. X-Ray Attenuation Property of the Au NPs versus Omnipaque

The X-ray attenuation properties of the synthesized TZ-PEG-Au NPs were compared to a conventional iodine-based molecular CT CA. The comparison included variations in the molar concentration of the contrast element (iodine or Au) and tube potentials (Omnipaque). CT phantom images of the aqueous suspensions showed that increasing the concentration of iodine or Au resulted in higher brightness in the CT images. In Figure 4a, 4b), it can be observed that the attenuation coefficients of the NPs were consistently higher than those of the conventional CA at all three energy levels. This indicates that the TZ-PEG-Au NPs possess superior X-ray attenuation properties, making them more effective in enhancing contrast in CT imaging compared to the iodine-based CA.

4. Discussion

The TEM images revealed that the synthesized TZ-PEG-Au NPs exhibited a quasi-spherical shape, with well-separated particles and small aggregates. In Figure 1a, a schematic diagram was presented to illustrate the structure of Au NPs covered with a PEG layer labeled with TZ. The analysis of the TEM results revealed that the final NPs exhibited a moderately identical size distribution. The TEM images showed that the NPs had a consistent shape and size across the sample. The average diameter of the NPs was measured to be

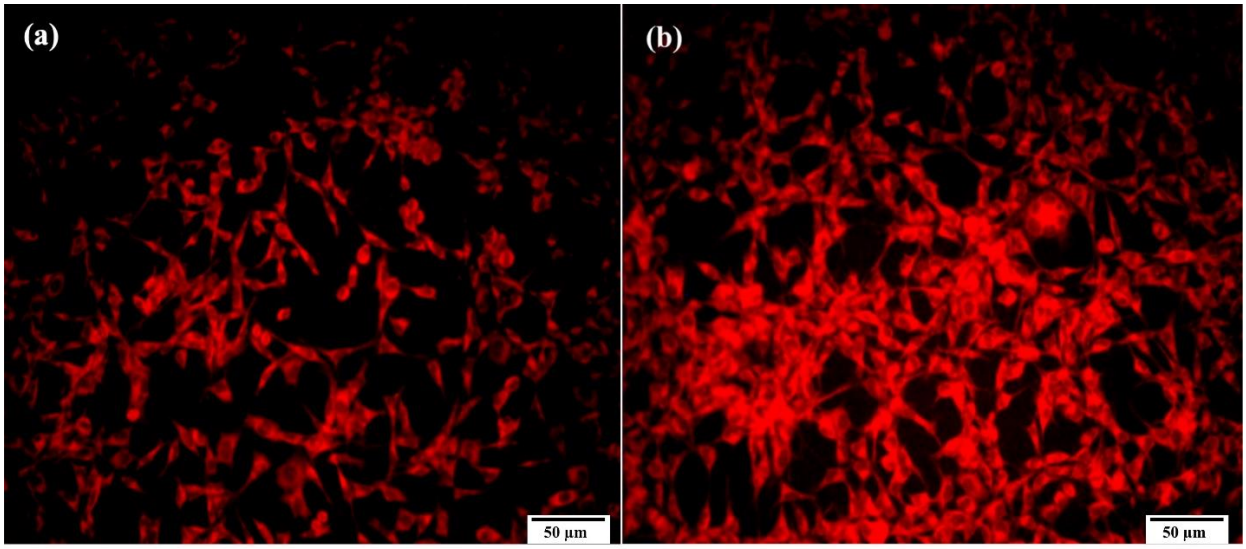

Figure 2. (a) Fluorescence microscopy images of Au NPs and (b) TZ-EG-Au NPs cell uptake after incubation with SKBr-3 cell lines after 4 h. Au (gold), PEG (polyethylene glycol), TZ (trastuzumab) and NPs (nanoparticles)

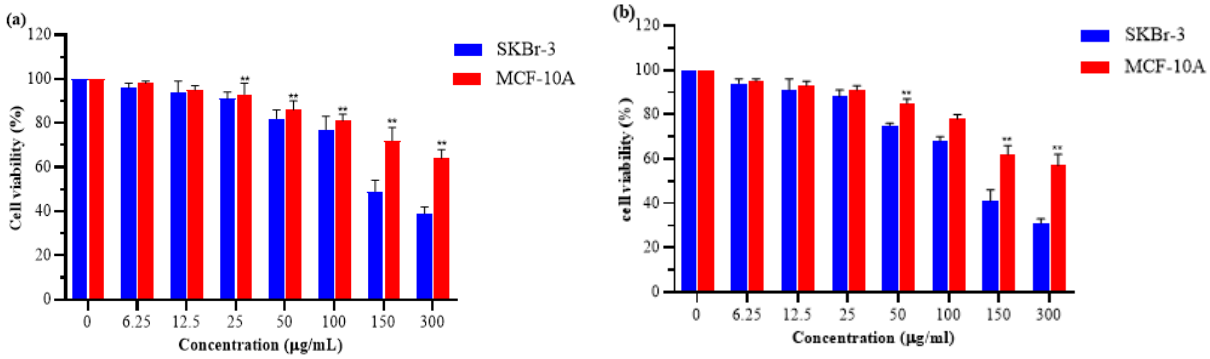

Figure 3. MTT assays of MCF-10A and SKBr-3 cells after treatment with TZ-PEG-Au NPs at various concentrations (0–300 μM) after 24 hours (a) and 48 hours (b) incubation. Au (gold), PEG (polyethylene glycol), TZ (trastuzumab) and NPs (nanoparticles)

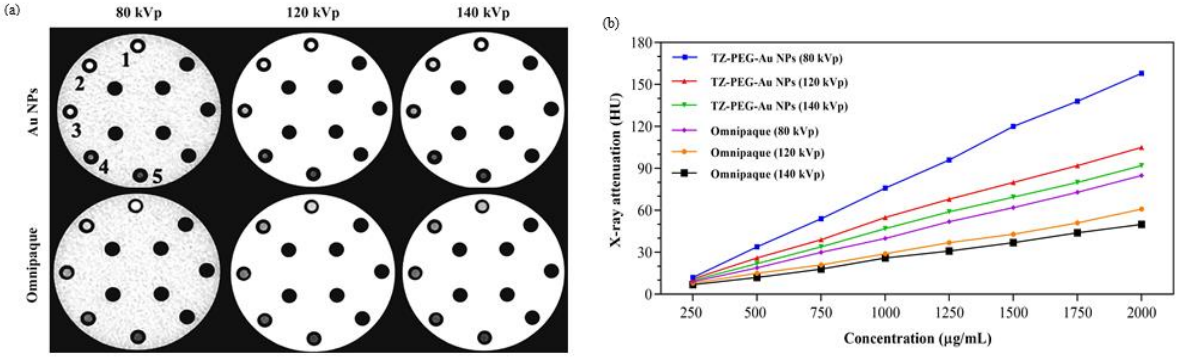

Figure 4. X-ray attenuation of TZ-PEG-Au NPs and Omnipaque in three X-ray tube potential (a) as a function of concentration (b). Au (gold), PEG (polyethylene glycol), TZ (trastuzumab) and NPs (nanoparticles)

approximately 45 nm. The size distribution of the NPs was within the desired range. The NPs' small size, below 100 nm, offers several advantages in their application. Firstly, NPs (under 100 nm) tend to exhibit high colloidal stability, minimizing aggregation or precipitation in solution. This stability is crucial for maintaining the NP's integrity and functionality during storage and administration. Secondly, the small size of the NPs confers several advantages, including the ability to exploit the Enhanced Permeation and Retention (EPR) effect. The EPR effect is a phenomenon commonly observed in tumor tissues, where leaky blood vessels and impaired lymphatic drainage allow for the accumulation of NPs within the tumor microenvironment. Due to their small size, the TZ-PEG-Au NPs can easily penetrate the leaky blood vessel walls surrounding the tumor and accumulate in the tumor tissue. This passive targeting strategy takes advantage of the EPR effect, allowing for selective accumulation of the NPs in the tumor while minimizing accumulation in healthy tissues [23]. Leveraging the EPR effect, the TZ-PEG-Au NPs have the potential to specifically accumulate in tumor tissues, enhancing their effectiveness as a targeted imaging agent. Moreover, the NPs' small size facilitates their delivery to tumor sites, as they can easily traverse the tumor vasculature and reach the target cells [24]. In the FTIR spectrum of Au NPs, a peak at approximately 530 cm-1 is observed, which can be assigned to the vibration of the Au atoms within the NPs [25]. The characteristic peaks witnessed around 580-682 cm^{-1} in the spectrum are likely attributed to the existence of H-O bending bands in the Au. These bending vibrations indicate the presence of Hydroxyl (OH) groups in the NPs. Additionally, absorption bands can be observed at 3410 cm^{-1}, which is indicative of stretching vibrations of OH groups [26].

Figure 2 demonstrated that the interaction between the TZ-PEGylated Au NPs and SKBr-3 cells was meaningfully improved compared to the non-modified NPs. Moreover, with increasing time of cell uptake, robust fluorescence intensity was perceived, indicating a higher uptake of the NPs by the cells. The increased cellular uptake is likely attributed to the specific ligand-receptor interactions between the PEGylated-TZ NPs

and the HER-2 receptors present on the SKBr-3 cell membrane. TZ, the targeting ligand used in this study, exhibits a high affinity for HER-2 receptors, facilitating the efficient internalization of the NPs into the cells. Furthermore, the encapsulation of the Au NPs within the PEGylated-TZ NPs further enhances their uptake by the cells [27]. This can be attributed to the increased labeling of TZ to HER-2 receptors, resulting in more effective cellular delivery of the TZ. The enhanced uptake of the PEGylated-TZ NPs demonstrated the advantages of specific targeting and improved internalization efficiency offered by this modification.

The results of the MTT analysis demonstrated that the cell viability decreased as the exposure time to the TZ-PEG-Au NPs increased. This decline in cell viability was particularly evident in SKBr-3 cells, which are BC cells. In contrast, the cytotoxicity of the NPs on MCF-10A cells, which are non-tumorigenic, was significantly lesser at all tested doses (P-value < 0.05). The observed difference in cytotoxicity between SKBr-3 and MCF-10A cells can be attributed to the differential expression of the TZ receptor. SKBr-3 cells exhibited higher levels of the HER-2 receptor compared to MCF-10A cells. The presence of a higher number of TZ receptors on SKBr-3 cells likely contributed to their increased susceptibility to the cytotoxic effects of the NPs. Importantly, the final NPs did not exert significant cytotoxicity on MCF-10A cells, even at high concentrations. This suggests that the NPs are relatively safe for non-tumorigenic cells, indicating their potential biocompatibility. The in-vitro outcomes depicted in Figure 3 support the biocompatibility of the NPs within the tested variety of 0-300 µM. The acceptable cell viability observed within this concentration range further suggests that the NPs can be used without causing significant harm to cells. These findings highlight the potential of TZ-PEG-Au NPs as a targeted contrast agent in biomedical applications, particularly for SKBr-3 BC cells with higher expression of the TZ receptor. Additional studies are required to evaluate the in-vivo biocompatibility and efficacy of the NPs, but the in-vitro results provide promising initial evidence for their suitability in such applications [28]. The study conducted by Babaye *et al.* demonstrated that increasing concentrations of TZ and TZ-coated NPs resulted in increased cytotoxic effects on the SKBr-3 cell line [13]. These findings are consistent with previously reported studies. Additionally, Cai *et al.* conducted an in vitro study assessing the cytotoxicity of TZ-Au NPs on the SKBr-3 cell line. They found that TZ-Au NPs had a significant binding affinity to SKBr-3 cells and were efficiently internalized compared to Au NPs. This increased internalization led to an increase in double-strand breaks in DNA. The study also reported a 55% decrease in cell viability in SKBr-3 cells when exposed to TZ-Au NPs. These findings highlight the potential cytotoxic effects of TZ and TZ-coated NPs on cancer cells, as well as their potential application in cancer treatments [29].

The quantitative measurements of CT values provided quantitative insights into the CT X-ray attenuation properties of both final NPs and CA. It was observed that the intensity of X-ray attenuation increased with higher concentrations of Au or iodine [30]. However, the increase in CT values for TZ-PEG-Au NPs was more significant compared to Omnipaque when the concentration of the CA (Au or iodine) was the same. The X-ray attenuation intensity of the final NPs was found to be approximately 1.4 times higher than that of Omnipaque at a concentration of 1500 g/mL and an X-ray energy of 120 kVp (Figure 4b). This information is presented in Figure 4, which illustrates the relative X-ray attenuation intensities of the NPs compared to Omnipaque. The enhanced contrast enhancement observed in the TZ-PEG-Au NPs compared to Omnipaque can be attributed to the higher X-ray attenuation coefficient of Au compared to iodine (the active component in Omnipaque). The X-ray attenuation coefficient is a measure of how strongly a material attenuates X-ray radiation. It depends on factors such as the electron density and atomic number of the material. Au has a higher electron density (19.32 g/cm^3) and atomic number (79) compared to iodine (4.9 g/cm^3 and 53, respectively). Due to its higher electron density and atomic number, Au exhibits stronger interactions with X-ray photons. When X-ray radiation passes through the TZ-PEG-Au NPs, the Au atoms have a higher probability of absorbing and scattering the X-ray photons. This results in a greater attenuation of the X-ray beam compared to the attenuation caused by iodine in Omnipaque [31]. Consequently, the final NPs exhibited superior CA properties, leading to improved contrast enhancement compared to Omnipaque. It is worth noting that as X-ray energy (kVp) rises, there is a tendency for decreased X-ray attenuation and contrast improvement due to better penetration of high-energy rays. However, the greater X-ray attenuation capability of final NPs compared to Omnipaque makes them particularly suitable for very sensitive CT imaging applications. The

present study would benefit from further research using an animal model and a larger sample size. Conducting in-vivo studies would provide a more realistic assessment of the behavior, biodistribution, and imaging performance of the TZ-PEG-Au NPs. Additionally, increasing the sample size would enhance the statistical power and generalizability of the findings, providing more robust and reliable results. These additions would strengthen the validity and applicability of the study, advancing its potential for translation into clinical practice. The study conducted by Khademi *et al.* focused on evaluating the effect of Au NPs with different shapes, sizes, surface chemistries, and concentrations on X-ray attenuation for CT imaging. The findings of the study indicated that smaller spherical Au NPs (13 nm) exhibited higher X-ray attenuation compared to larger ones (60 nm), suggesting their potential as effective CAts for CT imaging. The study also observed that the X-ray attenuation decreased when Au NPs were coated with PEG, which limited their aggregation. Furthermore, the study found that increasing the mass concentration of Au NPs led to an increase in X-ray attenuation. This information can be valuable for applications involving Au nanostructures for radiation dose enhancement, where NPs with high X-ray attenuation are utilized. Based on these findings, smaller spherical Au NPs were suggested as a potentially better alternative to Omnipaque, a commonly used CA for CT imaging [32].

In the study conducted by Tarighatnia *et al.*, the authors synthesized and characterized mesoporous silica-coated bismuth (MSBi) NPs conjugated with mucin-16 aptamer (MSBi@MUC16 NPs). These novel CAs were explored for their potential in detecting and quantifying cervical cancers using CT. The results obtained from both in-vitro and in-vivo experiments demonstrated that the targeted NPs exhibited a higher accumulation in overexpressing cells compared to non-targeted NPs, specifically in CT imaging modalities. Furthermore, in animal models, the targeted NPs showed efficient circulation in the bloodstream and selective accumulation at the HeLa tumor sites. These findings suggest the promising utility of MSBi@MUC16 NPs as effective CAs for CT imaging in the context of cervical cancer detection and diagnosis [33]. Also, Tarighatnia *et al.* developed Bi NPs coated with Dopamine (DOPA) as CT CAs. The Bi NPs were further functionalized with PEG and MUC-16 aptamer to create Bi-DOPA-PEG-I-MUC16 NPs. The study demonstrated that these NPs outperformed a commercial CA in terms of Contrast-to-Noise Ratio (CNR) and CT number. The Bi-DOPA-PEG-I-MUC16 NPs showed significantly higher CNR and CT numbers, approximately 8.9 and 13 times higher, respectively, at equivalent concentrations and similar radiation parameters [34].

5. Conclusion

In this study, the potential of modified Au NPs as a targeted CA for X-ray imaging in tumor diagnosis was investigated. The biocompatibility of Au NPs was confirmed as the viability of SKBr-3 cells remained unaffected by different doses of the NPs. CT imaging of Breast Cancer (BC) cells was successfully achieved after incubation with Au NPs, indicating their ability to facilitate targeted imaging. Compared to the traditional CA (Omnipaque), the presence of Au NPs led to higher X-ray attenuation, suggesting their potential for efficient CT imaging of human BC cells. The concentration of Au NPs and the duration of incubation were found to significantly influence X-ray attenuation, suggesting that optimization of these factors can enhance CT contrast and improve imaging outcomes. Significantly, targeted Au NPs exhibited a greater increase in Hounsfield Units (HU) compared to Omnipaque, indicating their superior contrast enhancement capability. At certain concentrations, the CT values of targeted cells were approximately three times higher than those incubated with Omnipaque. These findings highlight the promising clinical applications of targeted Au NPs as a safe and effective CA for CT imaging. Further research and optimization are warranted to fully explore and harness the potential of targeted Au NPs in clinical settings.

References

1- Ahmed M Afifi, Anas M Saad, Muneer J Al-Husseini, Ahmed Osama Elmehrath, Donald W Northfelt, and Mohamad Bassam Sonbol, "Causes of death after breast cancer diagnosis: A US population-based analysis." *Cancer,* Vol. 126 (No. 7), pp. 1559-67, (2020).

2- Zeinab Safarpour Lima, Mohammad Reza Ebadi, Ghazaleh Amjad, and Ladan Younesi, "Application of imaging technologies in breast cancer detection: a review article." *Open Access Macedonian Journal of Medical Sciences,* Vol. 7 (No. 5), p. 838, (2019).

3- Dolatkhah M Hashemzadeh N, Adibkia K, Aghanejad A, Barzegar-Jalali M, Omidi Y, Barar J, "Recent advances in breast cancer immunotherapy: The promising impact of

nanomedicines." *Life Sciences,* Vol.;271:119110(2021 Apr 15).

4- Tarighatnia A Kadkhoda J, Tohidkia MR, Nader ND, Aghanejad A., "Photothermal therapy-mediated autophagy in breast cancer treatment: Progress and trends. *Life sciences*. 2022 Jun 1;298:120499.".

5- Luca Volterrani *et al.*, "Dual-energy CT for locoregional staging of breast cancer: preliminary results." *American Journal of Roentgenology,* Vol. 214 (No. 3), pp. 707-14, (2020).

6- Ali Tarighatnia, Gurkaran Johal, Ayuob Aghanejad, Hossein Ghadiri, and Nader D Nader, "Tips and tricks in molecular imaging: a practical approach." *Frontiers in Biomedical Technologies,* Vol. 8 (No. 3), pp. 226-35, (2021).

7- Hedieh Mansouri *et al.*, "A biocompatible theranostic nanoplatform based on magnetic gadolinium-chelated polycyclodextrin: in vitro and in vivo studies." *Carbohydrate Polymers,* Vol. 254p. 117262, (2021).

8- Ziyaee S, Malekzadeh R, Ghorbani M, Nasiri Motlagh B, Asghariazar V, and Mortezazadeh T, "Preparation of MnO2@ poly-(DMAEMA-co-IA)-conjugated methotrexate nano-complex for MRI and radiotherapy of breast cancer application." *Magnetic Resonance Materials in Physics, Biology and Medicine,* Vol. 36(5):779-95(2023).

9- Behnaz Babaye Abdollahi *et al.*, "Main approaches to enhance radiosensitization in cancer cells by nanoparticles: A systematic review." *Advanced Pharmaceutical Bulletin,* Vol. 11 (No. 2), p. 212, (2021).

10- Tarighatnia A Jamshidi N, Ghaziyani MF, Sajadian F, Nader ND, " Folic acid-conjugated Fe-Au-based nanoparticles for dual detection of breast cancer cells by magnetic resonance imaging and computed tomography." *Frontiers in Biomedical Technologies,* Vol.;11(1):122-9(2024).

11- Reza Malekzadeh *et al.*, "Nanoarchitecture-based photothermal ablation of cancer: a systematic review." *Environmental Research,* p. 116526, (2023).

12- Tarighatnia A Mohaghegh S, Omidi Y, Barar J, Aghanejad A, Adibkia K., "Multifunctional magnetic nanoparticles for MRI-guided co-delivery of erlotinib and L-asparaginase to ovarian cancer." *Journal of Microencapsulation.,* (2022 May 19;39(4):394-408.).

13- Behnaz Babaye Abdollahi, Marjan Ghorbani, Hamed Hamishehkar, Reza Malekzadeh, and Alireza Farajollahi, "Synthesis and characterization of actively HER-2 Targeted Fe3O4@ Au nanoparticles for molecular radiosensitization of breast cancer." *BioImpacts: BI,* Vol. 13 (No. 1), p. 17, (2023).

14- Eun Hye Jeong, Giyoung Jung, Cheol Am Hong, and Hyukjin Lee, "Gold nanoparticle (AuNP)-based drug delivery and molecular imaging for biomedical applications." *Archives of pharmacal research,* Vol. 37pp. 53-59, (2014).

15- Wen S Li K, Larson AC, Shen M, Zhang Z, Chen Q, Shi X, Zhang G., "Multifunctional dendrimer-based nanoparticles for in vivo MR/CT dual-modal molecular imaging of breast cancer." *International journal of nanomedicine,* Vol. 19:2589-600, (2013 Jul).

16- Petersen W Rayavarapu RG, Ungureanu C, Post JN, van Leeuwen T, Manohar S, "Synthesis and bioconjugation of gold nanoparticles as potential molecular probes for light-based imaging techniques." *International Journal of biomedical imaging,* Vol. 29817-1, (2007).

17- Hsu JC Bouché M, Dong YC, Kim J, Taing K, Cormode DP, "Recent advances in molecular imaging with gold nanoparticles." *Bioconjugate chemistry.,* Vol. 4;31(2):303-14, (2019 Nov).

18- Iqbal N. Iqbal N, "Human epidermal growth factor receptor 2 (HER2) in cancers: overexpression and therapeutic implications." *Molecular biology international.,* Vol. 2014.(2014).

19- Shastry M Swain SM, Hamilton E, "Targeting HER2-positive breast cancer: advances and future directions." *Nature reviews Drug discovery,* Vol. 22(2):101-26. (2023 Feb).

20- Malekzadeh R, Babaye Abdollahi B, Ghorbani M, Pirayesh Islamian J, and Mortezazadeh T, "Trastuzumab conjugated PEG–Fe3O4@ Au nanoparticle as an MRI biocompatible nano-contrast agent." *International Journal of Polymeric Materials and Polymeric Biomaterials,* Vol. 3;72(10):759-70. (2023).

21- Motiei M Reuveni T, Romman Z, Popovtzer A, Popovtzer R., "Targeted gold nanoparticles enable molecular CT imaging of cancer: an in vivo study." *International journal of nanomedicine.,* Vol. 11:2859-64. (2011 Nov).

22- Lisha KP, Anshup, and Pradeep T, "Enhanced visual detection of pesticides using gold nanoparticles." *Journal of Environmental Science and Health Part B,* Vol. 16;44(7):697-705, (2009 Sep).

23- Mahmoudi G Tarighatnia A, Kiani M, Nader ND, "Current Challenges and New Opportunities of Hybrid Nanoparticles for Diagnosis and Treatment of Cancer." *Frontiers in Biomedical Technologies,* Vol. 1;11(1):1-5(2024 Jan).

24- Owoseni O Ejigah V, Bataille-Backer P, Ogundipe OD, Fisusi FA, Adesina SK, "Approaches to improve macromolecule and nanoparticle accumulation in the tumor microenvironment by the enhanced permeability and retention effect." *Polymers,* Vol. Jun 27;14(13):2601(2022).

25- Deb MK Khalkho BR, Kurrey R, Sahu B, Saha A, Patle TK, Chauhan R, Shrivas K., "Citrate functionalized gold nanoparticles assisted micro extraction of L-cysteine in milk and water samples using Fourier transform infrared

spectroscopy " *Spectrochimica Acta Part A: Molecular and Biomolecular Spectroscopy,* Vol. 15;267:120523.(2022 Feb).

26- Suriyakala G Sathiyaraj S, Gandhi AD, Babujanarthanam R, Almaary KS, Chen TW, Kaviyarasu K., "Biosynthesis, characterization, and antibacterial activity of gold nanoparticles." *Journal of Infection and Public Health,* Vol. 1;14(12):1842-7(2021 Dec).

27- Merdan T Germershaus O, Bakowsky U, Behe M, Kissel T, "Trastuzumab− polyethylenimine− polyethylene glycol conjugates for targeting Her2-expressing tumors." *Bioconjugate Chemistry,* Vol. 20;17(5):1190-9(2006 Sep).

28- Tohidkia MR Siminzar P, Eppard E, Vahidfar N, Tarighatnia A, Aghanejad A., "Recent trends in diagnostic biomarkers of tumor microenvironment." *Molecular Imaging and Biology,* (2023 Jun;25(3):464-82.).

29- Chattopadhyay N Cai Z, Yang K, Kwon YL, Yook S, Pignol JP, Reilly RM., "111In-labeled trastuzumab-modified gold nanoparticles are cytotoxic in vitro to HER2-positive breast cancer cells and arrest tumor growth in vivo in athymic mice after intratumoral injection. Nuclear medicine and biology. 2016 Dec 1;43(12):818-26.".

30- Saung MT Galper MW, Fuster V, Roessl E, Thran A, Proksa R, Fayad ZA, Cormode DP., " Effect of computed tomography scanning parameters on gold nanoparticle and iodine contrast." *Investigative radiology,* Vol. 1;47(8):475-81(2012 Aug).

31- Kim EM Kim SH, Lee CM, Kim DW, Lim ST, Sohn MH, Jeong HJ, "Synthesis of PEG-iodine-capped gold nanoparticles and their contrast enhancement in in vitro and in vivo for X-ray/CT." *Journal of Nanomaterials,* Vol. 1;2012:46(2012 Jan).

32- Sarkar S Khademi S, Kharrazi S, Amini SM, Shakeri-Zadeh A, Ay MR, Ghadiri H., "Evaluation of size, morphology, concentration, and surface effect of gold nanoparticles on X-ray attenuation in computed tomography. Physica Medica. 2018 Jan 1;45:127-33.".

33- Abdkarimi MH Tarighatnia A, Nader ND, Mehdipour T, Fouladi MR, Aghanejad A, Ghadiri H., " Mucin-16 targeted mesoporous nano-system for evaluation of cervical cancer via dual-modal computed tomography and ultrasonography. *New journal of chemistry*." (2021;45(40):18871-80.).

34- Fouladi MR Tarighatnia A, Tohidkia MR, Johal G, Nader ND, Aghanejad A, Ghadiri H., "Engineering and quantification of bismuth nanoparticles as targeted contrast agent for computed tomography imaging in cellular and animal models." *Journal of drug delivery science and technology,* (2021 Dec 1;66:102895.).